Test of the superdiffusion model in the interstellar medium around the Geminga pulsar

Sheng-Hao Wang,[1,2] Kun Fang,[1,*] Xiao-Jun Bi,[1,2,†] and Peng-Fei Yin[1]

[1]*Key Laboratory of Particle Astrophysics, Institute of High Energy Physics, Chinese Academy of Science, Beijing 100049, China*

[2]*University of Chinese Academy of Sciences, Beijing 100049, China*

(Received 15 January 2021; accepted 4 March 2021; published 24 March 2021)

Cosmic-ray (CR) propagation in the interstellar medium (ISM) of the Galaxy might be a superdiffusion process, rather than the commonly adopted normal diffusion. The spatial distribution of CRs around a pointlike source can be adopted to test the real picture that describes the CR propagation. The TeV γ-ray halo around the Geminga pulsar is an ideal target, where the spatial distribution of the escaped electrons and positrons can be derived from the morphology of the halo. In this work, we test the superdiffusion model in the ISM around the Geminga pulsar by fitting it to the surface brightness profile of the Geminga halo measured by HAWC. Our results show that the chi-square statistic monotonously increases as α decreases from 2 to 1, where α is the characteristic index of superdiffusion describing the degree of fractality of the ISM and $\alpha = 2$ corresponds to the normal diffusion model. We find that a model with $\alpha < 1.32$ (using the data within 4° around the pulsar) or $\alpha < 1.4$ (using the data within 6° around the pulsar) is disfavored at 95% confidence level. A superdiffusion model with α close to 2 can well explain the morphology of the Geminga halo, while it predicts much higher positron flux at Earth than the normal diffusion model. This has important implication for the interpretation of the CR positron excess.

DOI: 10.1103/PhysRevD.103.063035

I. INTRODUCTION

Several middle-aged pulsars, such as the Geminga pulsar, are reported to be surrounded by TeV γ-ray halos with scales larger than 20 pc [1,2]. These γ-ray halos are generated by free electrons and positrons[1] diffusing out from the corresponding pulsar wind nebulae (PWNe), rather than being interpreted by γ-ray PWNe [3]. According to the evolution model of the PWN, the original PWNe of the middle-aged pulsars were broken a long time ago [4]. These pulsars are currently traveling in the interstellar medium[2] (ISM) and driving bow-shock PWNe with scales $\lesssim$1 pc. This is consistent with the observations of the x-ray PWN of the Geminga pulsar [6–8]. These TeV γ-ray halos are generated mainly through the inverse Compton scattering (ICS) of the homogeneous cosmic microwave background, so the morphologies of the halos unambiguously indicate how electrons propagate in the ISM.

Cosmic-ray (CR) propagation in the ISM is usually modeled by the diffusion process considering the turbulent nature of the ISM [9]. The diffusion approximation is based on the assumption that the inhomogeneity of the chaotic magnetic field has small-scale character and is negligible in terms of the scale of interest. However, multiscale inhomogeneities could exist in the ISM. The ISM is more likely to be a fractal type and the normal diffusion can be generalized to superdiffusion [10–13], where the CR propagation is simulated by Lévy flights instead of the Brownian motion. This model has been applied in the Galactic-scale propagation of CRs to explain features of the CR energy spectra [10,14], and also in the mechanism of shock acceleration [15,16]. In this work, we test the superdiffusion model in a localized region of the Galaxy by explaining the morphology of the Geminga halo. As the diffusion packets are different for the normal diffusion and superdiffusion models, the γ-ray morphologies predicted by them could also be distinct.

This paper is organized as follows. In Sec. II, we introduce the superdiffusion model and the solution of the propagation equation. Then we briefly introduce the information of Geminga in Sec. III. We fit the γ-ray surface brightness profile (SBP) of the Geminga halo measured by HAWC with different propagation models and discuss the fitting results in Sec. IV. In Sec. V we discuss the impact on the interpretation of the positron excess according to the results of Sec. IV. Finally, we conclude in Sec. VI.

*fangkun@ihep.ac.cn

†bixj@ihep.ac.cn

[1]*Electrons* will denote both electrons and positrons hereafter.

[2]The pulsars could also be inside their old host SNRs if the SNRs are large enough [5].

II. THE SUPERDIFFUSION MODEL

After escaping from the source, CRs are continuously scattered by the chaotic magnetic field in the ISM. If the chaotic magnetic field is uniformly distributed, the particle transport can be simulated by the Brownian motion [9]. However, the realistic magnetic field in the ISM may consist of turbulent and relatively regular components, where very long jumps for CRs are permitted. Lévy flight, which is characterized by occasionally very long steps, should be the more proper description in this case [10–13]. For one-dimensional Lévy flight, the probability density function (PDF) of the individual step length x has the heavy-tailed form of $P(x) \propto |x|^{-1-\alpha}$ for $x \to \infty$, where $0 < \alpha < 2$. Obviously, the variance of the step length is infinite, which is different from that of the Brownian motion. The widening of the diffusion packet with time is also faster for Lévy flight ($\propto t^{1/\alpha}$) than the normal diffusion case ($\propto t^{1/2}$), so this scenario is named after superdiffusion or accelerated diffusion [12].

As the PDF of Lévy flight can be described by the fractional Laplacian equation, the propagation equation of CR electrons should be

$$\frac{\partial N(E,\boldsymbol{r},t)}{\partial t} = -D(E,\alpha)(-\Delta)^{-\frac{\alpha}{2}}N(E,\boldsymbol{r},t) + \frac{\partial[b(E)N(E,\boldsymbol{r},t)]}{\partial E} + Q(E,\boldsymbol{r},t), \quad (1)$$

where N is the differential number density of electrons, D is the diffusion coefficient, and Q is the source function for which we will present the details in Sec. III. The index α represents the degree of fractality of the ISM and for $\alpha = 2$ the equation degenerates to the normal diffusion case. The radiative energy-loss rate $b(E) = b_0E^2$ induced by synchrotron radiation and ICS must be considered for high-energy electrons. The magnetic field strength is assumed to be 3 μG in the synchrotron term. For the ICS process, we adopt the seed photon field in Ref. [1] and the parametrization given by Ref. [17] to calculate the energy-loss rate, where the Klein-Nishina correction is accurately considered.

We solve Eq. (1) with the Green's function method. The Green's function takes the form of

$$G(E,\boldsymbol{r},t;E_0,\boldsymbol{r}_0,t_0) = \frac{\rho_3^{(\alpha)}(|\boldsymbol{r}-\boldsymbol{r}_0|\lambda^{-1/\alpha})}{b(E)\lambda^{3/\alpha}}\delta(t-t_0-\tau)H(\tau), \quad (2)$$

where

$$\tau = \int_E^{E_0}\frac{dE'}{b(E')}, \qquad \lambda = \int_E^{E_0}\frac{D(\alpha,E')}{b(E')}dE', \quad (3)$$

and H is the Heaviside step function. In Eq. (2) $\rho_3^{(\alpha)}(r)$ is the PDF of a three-dimensional spherically symmetrical stable distribution with index α. The exact expression of $\rho_3^{(\alpha)}(r)$ is

$$\rho_3^{(\alpha)}(r) = \frac{1}{2\pi^2 r}\int_0^\infty e^{k^\alpha}\sin(kr)kdk, \quad (4)$$

while in practice it can be expressed with convergent and asymptotic series [18]:

$$\rho_3^{(\alpha)}(r) = \frac{1}{2\pi^2\alpha}\sum_{n=0}^{\infty}\frac{(-1)^n}{(2n+1)!}\Gamma\left(\frac{2n+3}{\alpha}\right)r^{2n}, \quad (5)$$

$$\rho_3^{(\alpha)}(r) = \frac{1}{2\pi^2 r}\sum_{n=1}^{\infty}\frac{(-1)^{n-1}}{n!}\Gamma(n\alpha+2)\sin\left(\frac{n\alpha\pi}{2}\right)r^{-n\alpha-2}. \quad (6)$$

We show $\rho_3^{(\alpha)}(r)$ in Fig. 1, where we can clearly see the differences between the heavy-tailed distributions for $\alpha < 2$ and the Gaussian distribution for $\alpha = 2$. The solution of Eq. (1) can then be expressed as

$$\begin{aligned} N(E,\boldsymbol{r},t) &= \int_{R^3}d^3\boldsymbol{r}_0\int_{-\infty}^{t}dt_0\int_{-\infty}^{+\infty}dE_0G(E,\boldsymbol{r},t;E_0,\boldsymbol{r}_0,t_0)Q(E_0,\boldsymbol{r}_0,t_0) \\ &= \int_{R^3}d^3\boldsymbol{r}_0\int_{t-1/(b_0E)}^{t}dt_0\frac{b(E_\star)}{b(E)}\frac{\rho_3^{(\alpha)}(|\boldsymbol{r}-\boldsymbol{r}_0|\lambda^{-1/\alpha})}{\lambda^{3/\alpha}}Q(E_\star,\boldsymbol{r}_0,t_0), \end{aligned} \quad (7)$$

where $E_\star \simeq E/[1-b_0E(t-t_0)]$.

From Eq. (7), we can get the electron number density at an arbitrary distance from a pulsar. To calculate the γ-ray SBP around the pulsar, we integrate the electron number density along the line of sight from the Earth to the vicinity of the pulsar and get the electron surface density at an arbitrary angular distance θ from the pulsar:

$$F(\theta) = \int_0^{+\infty}N(l_\theta)dl_\theta, \quad (8)$$

where l_θ is the length in that line of sight, and $N(l_\theta)$ is the electron number density at a distance of $\sqrt{d^2+l_\theta^2-2dl_\theta\cos\theta}$ from the pulsar, where d is the

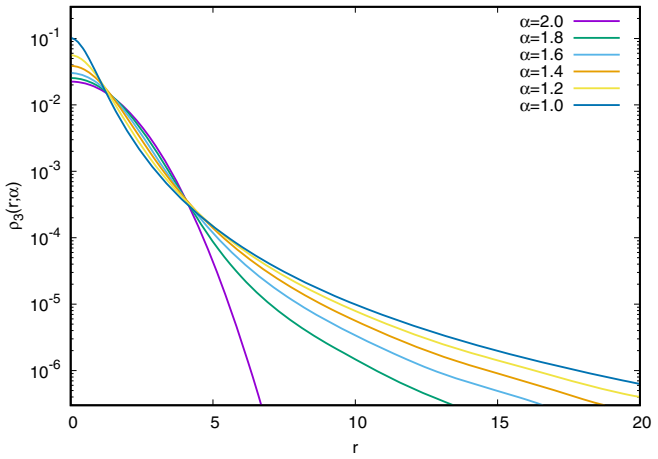

FIG. 1. Probability density functions of three-dimensional spherically symmetric stable distributions for different α.

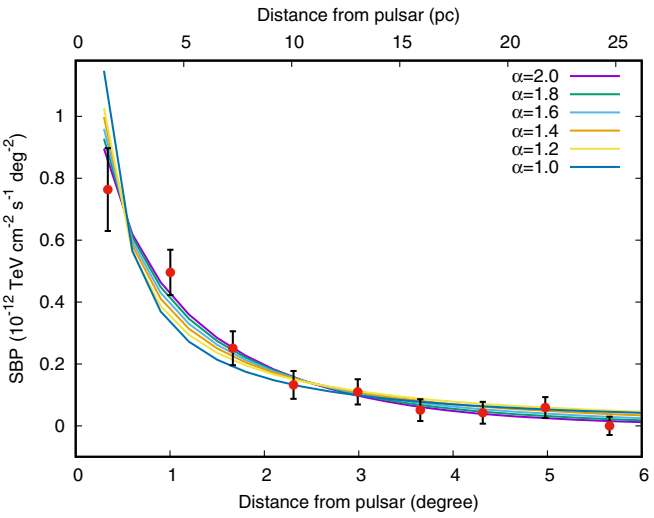

FIG. 2. Best-fit surface brightness profiles to the HAWC data [1] with the normal diffusion model ($\alpha = 2$) and superdiffusion models ($\alpha < 2$).

distance between the pulsar and the Earth. With $F(\theta)$ and the standard calculation of ICS [19], we can finally obtain the γ-ray SBP around the pulsar.

III. THE SOURCE GEMINGA

The Geminga halo is so far the best-studied TeV halo. The γ-ray SBP is precisely measured by HAWC [1] and is an ideal target to investigate the propagation of CR electrons. In the normal diffusion scenario, the derived diffusion coefficient around the Geminga pulsar is more than 2 orders of magnitude smaller than the average value in the Galaxy indicated by the boron-to-carbon ratio [20]. The origin of the slow diffusion has been discussed in recent works [5,21,22].

The parameters of the Geminga pulsar can be obtained from the Australia Telescope National Facility catalog [23]. The age of the pulsar is $t_s = 342$ kyr and the current spin-down luminosity is $L = 3.25 \times 10^{34}\,\mathrm{erg\,s^{-1}}$. The latest version of the catalog gives the pulsar distance as $d = 190$ pc and provides the reference, Ref. [24], where the distance is derived with the optical measurement of the trigonometric parallax. However, the distance given by Ref. [24] is 157 pc rather than 190 pc. Here we adopt $d = 250$ pc which is determined by the latest parallax measurement [25].

Electrons are accelerated to very high energy inside the Geminga PWN. As the scale of the Geminga PWN is significantly smaller than the TeV halo, it is reasonable to assume it to be a point source. The time dependency of the electron injection is assumed to be proportional to the spin-down luminosity of the pulsar as $\propto (1 + t/t_{\rm sd})^{-2}$, where $t_{\rm sd}$ is the spin-down time scale of pulsar. We set a typical value of $t_{\rm sd} = 10$ kyr. As the cooling time of 100 TeV electrons is about 10 kyr, the parent electrons of the present TeV γ-ray halo are generated in the very recent age of Geminga. So the value of $t_{\rm sd}$ impacts little on the time profile as $t/t_{\rm sd} \gg 1$. The injection energy spectrum can be described by a power law within the energy range of interest as $\propto E^{-p}$. We adopt $p = 2.24$ which is measured by the HAWC work [1]. Thus, the source term can be written as

$$Q(E, \boldsymbol{r}, t) = \begin{cases} Q_0 (E/E_{100})^{-p} \delta(\boldsymbol{r} - \boldsymbol{r}_s)[(t_s + t_{\rm sd})/(t + t_{\rm sd})]^2, & t > 0 \\ 0, & t < 0, \end{cases} \tag{9}$$

where $\boldsymbol{r}_s$ is the position of the pulsar and we set the birth time of the pulsar to be the zero point of time. The constant Q_0 is the current-time normalization at the energy of $E_{100} = 100$ TeV.

IV. FIT TO THE HAWC DATA

We test the superdiffusion propagation in the regime of $1 \le \alpha \le 2$ by fitting it to the γ-ray SBP of HAWC [1]. For each α, we seek the best-fit model by minimizing the chi-square statistic χ^2 between the model and the data points. The NLopt[3] package and the optimization algorithm BOBYQA [26] are adopted for the fitting procedures. The free parameters are the anomalous diffusion coefficient D and the constant factor of the source term Q_0. Since HAWC provides the SBP in a single energy bin of 8–40 TeV which

[3] http://github.com/stevengj/nlopt

TABLE I. Best-fit parameters for the HAWC data (using the data within 4° around the Geminga pulsar).

α	2.0	1.8	1.6	1.4	1.2	1.0
$\log_{10}[D(\mathrm{cm}^{\alpha}\,\mathrm{s}^{-1})]$	27.4	23.6	19.9	16.3	12.7	9.1
$Q_0(10^{28}\ \mathrm{TeV}^{-1}\,\mathrm{s}^{-1})$	2.5	2.9	3.5	4.8	9.2	15.6

is not very broad, we assume an energy-independent D in the calculations.

HAWC measures the SBP within 10° around the Geminga pulsar. However, we do not use all the SBP data in the fitting procedures as the data at large angular distances could be affected by other potential γ-ray sources. As indicated by Fig. 1, the differences of particle distribution between the propagation models are still significant at large distances from the source. If we include the data at large angular distances, the χ^2 test may be disturbed by the inhomogeneous γ-ray background. We use the data within $\theta_{\mathrm{max}} = 4°$ (≈17 pc) around the pulsar as a benchmark and test the case of $\theta_{\mathrm{max}} = 6°$ (≈26 pc) for comparison.

The fitting results are presented in Fig. 2 and the best-fit parameters are listed in Table I. Superdiffusion models with $\alpha \lesssim 1.5$ yield too steep inner profiles of the γ-ray halo as can be seen in Fig. 2. Due to the nature of Lévy flight, the superdiffusion models predict steeper profiles close to the source and flatter profiles far from the source in comparison with the normal diffusion case. If the inner fluxes are forced to fit the data for the superdiffusion models, the outer fluxes will be much higher than the data. The reduced χ^2 (χ^2 divided by degrees of freedom) monotonously increases as α decreases from 2 to 1, which is shown in the left panel of Fig. 3. The results indicate that the normal diffusion model is still the best depiction among the diffusion scenarios in terms of the current measurement.

We then provide a quantitative constraint on α by assuming it as a variable parameter and deriving its one-dimensional distribution. According to the Bayesian inference, we have $P(\alpha) \propto L(\alpha) \propto \exp[-\chi^2(\alpha)/2]$, where $P(\alpha)$ is the posterior PDF and $L(\alpha)$ is the likelihood function. The relative probability densities can be then derived at the knots where $\chi^2(\alpha)$ are available. We create a PDF with the form of

$$P(\alpha) = c_0\left\{\exp\left[-\frac{(\alpha - c_1)^2}{2c_2^2}\right] - \exp\left(-\frac{c_1^2}{2c_2^2}\right)\right\} \quad (10)$$

to fit the relative probability densities, where c_0, c_1, and c_2 are free parameters. The expression ensures $P(0) = 0$ since the domain of α is (0,2] [27]. We determine the free parameters by the least square method and then rescale c_0 to satisfy the normalization condition $\int_0^2 P(\alpha)d\alpha = 1$. The obtained PDFs are shown in the right panel of Fig. 3 with solid lines. The points in the figure are the relative probability densities used for the fits, which are rescaled after normalizing $P(\alpha)$. The best-fit parameters are $c_0 = 2.69$, $c_1 = 2.11$, and $c_2 = 0.383$ for the case of $\theta_{\mathrm{max}} = 4°$ and $c_0 = 3.13$, $c_1 = 2.12$, and $c_2 = 0.349$ for the case of $\theta_{\mathrm{max}} = 6°$. Finally, we exclude $\alpha < 1.32$ for the former case and $\alpha < 1.40$ for the latter at 95% confidence level (C.L.).

V. IMPACT ON THE POSITRON EXCESS

The Geminga pulsar was considered as one of the best candidate sources of the CR positron excess [28–30]. However, if the slow diffusion measured by HAWC pervades the ISM between Geminga and the solar system, Geminga can hardly contribute to the positron flux at Earth as the positrons do not have enough time to reach the Earth [1]. This problem will be alleviated if the slow diffusion only happens in the nearby ISM of the Geminga pulsar [31–34]. On the other hand, it is possible that the diffusion

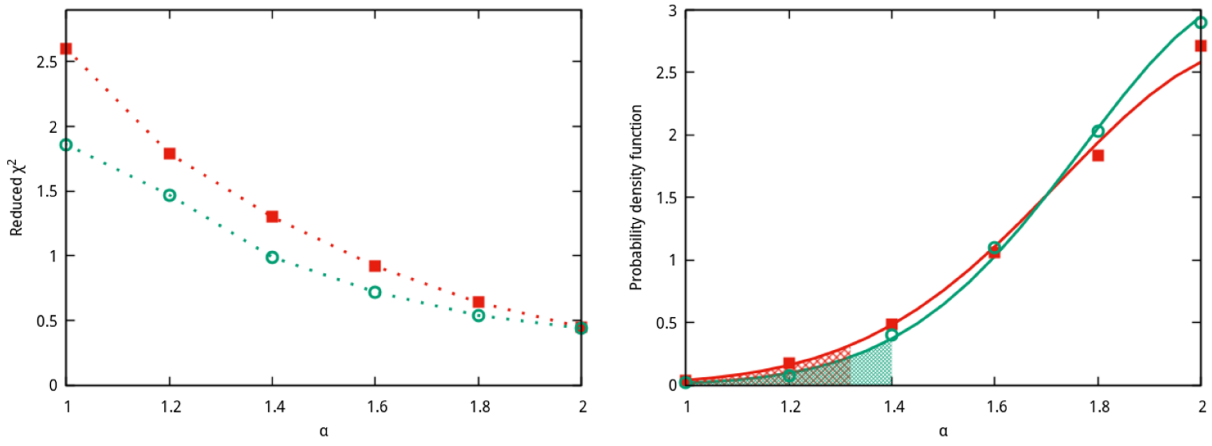

FIG. 3. Left: reduced χ^2 of the fitting procedures for different assumptions of α. The red filled squares correspond to the results in Fig. 2 where the HAWC data within 4° around the pulsar are used. The case using the data within 6° is shown with the green empty circles. Right: the corresponding probability density functions of α derived with $\chi^2(\alpha)$. The shaded areas show the intervals at 5% C.L.

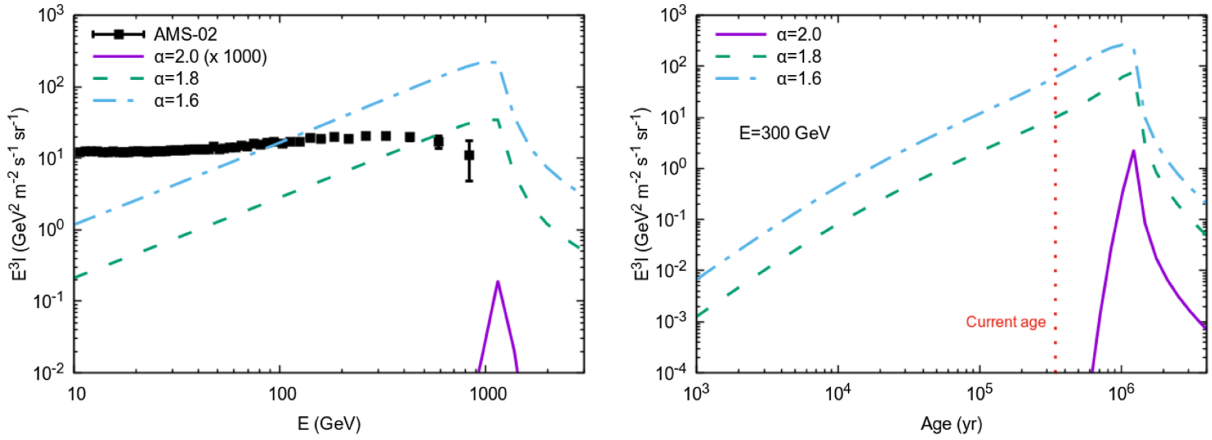

FIG. 4. Left: positron spectra at Earth contributed by Geminga with both the normal diffusion model and superdiffusion models. The parameters are adopted from Table I, which are derived from the HAWC measurement of the Geminga halo. The AMS-02 positron spectrum is also shown for comparison [37]. Right: positron fluxes from Geminga at 300 GeV as functions of the pulsar age, corresponding to the models in the left panel.

coefficient in the Galactic disk is generally much smaller than the average value in the Galaxy [35,36].

The discussion in the above paragraph is based on the normal diffusion model. The results in Sec. IV indicate that a superdiffusion model with $\alpha > 1.4$ is permitted by the current measurement. As can be seen in Fig. 1, superdiffusion models yield much higher fluxes at a large distance from the source than the normal diffusion due to the heavy-tailed distribution. We assume a one-zone superdiffusion scenario to calculate the positron flux from Geminga. The left panel of Fig. 4 shows the positron spectra in the cases of $\alpha = 2.0$, $\alpha = 1.8$, and $\alpha = 1.6$ adopting the parameters in Table I. The diffusion coefficient is extrapolated from the value in the HAWC energy range with the relation of $D \propto E^{1/3}$, which is predicted by Kolmogorov's theory. As expected, Geminga can contribute significant positron flux in comparison with the AMS-02 data [37] in the superdiffusion models, without the assumption of two-zone propagation mentioned above. More intuitively, we show the positron fluxes from Geminga at 300 GeV as functions of the pulsar age in the right panel of Fig. 4. Positrons come much faster to the Earth in the superdiffusion models with power-law-like time dependencies, rather than the steep time dependency of $\sim \exp[-r^2/(4Dt)]$ in the normal diffusion model. The flux cutoff above 10^6 yr is due to the radiative cooling of 300 GeV positrons.

Note we still adopt $p = 2.24$ in the above calculations, which are derived with the TeV observation of HAWC. As the AMS-02 positron spectrum is in the GeV range, it is more reasonable to use the Fermi-LAT observation of Geminga to constrain the injection spectrum and diffusion coefficient in the same energy range [38,39]. However, the constraint from Fermi-LAT is model dependent and the analysis is beyond the scope of this work.

VI. CONCLUSION

In this work, we test the superdiffusion model in the ISM around the Geminga pulsar by fitting it to the SBP measured by HAWC. This model depicts particle propagation in a fractal medium with Lévy flight, which could be a more appropriate model to describe the intricate magnetic field in the ISM than the normal diffusion model. The Lévy flight superdiffusion is expressed by the fractional Laplacian in the propagation equation with the order of $\alpha/2$, where $\alpha \in (0, 2)$. Through the χ^2 test, we find that the normal diffusion ($\alpha = 2$) still gives the best fit to the HAWC data. The reduced χ^2 monotonously increases with the decrease of α and a model with $\alpha < 1.32$ ($\theta_{\rm max} = 4°$) or $\alpha < 1.4$ ($\theta_{\rm max} = 6°$) is disfavored at 95% C.L. A model with small α gives poor fit to the γ-ray fluxes close to the pulsar. With more TeV halos being accurately measured in the coming future, particle propagation in localized regions of the Galaxy can be further constrained.

A superdiffusion model with $\alpha > 1.4$ is still permitted by the current measurement of the Geminga halo. Models with α close to 2 can give comparable fitting results to that of the normal diffusion model, however, they predict distinct positron spectra at Earth. Due to the nature of the heavy-tailed distribution of the superdiffusion model, part of the positrons come much faster to the Earth and the positron flux from Geminga is much higher than that predicted by the normal diffusion model. In contrast to the conclusion in Ref. [1], Geminga could have a significant contribution to the observed high-energy positron spectrum in the superdiffusion scenario even if the small diffusion coefficient measured around the Geminga pulsar is applied in the whole region between Geminga and the Earth.

The test may also provide information on the origin of the inefficient particle propagation in TeV halos. For example, it has been proposed that the slow-diffusion zone

around the Geminga pulsar may be due to its crushed relic PWN [33,34]. Considering the filamentary structures in the relic PWN due to Rayleigh-Taylor instabilities [40], this scenario may be described by the superdiffusion model with α significantly smaller than 2, which can then be tested by the method depicted in this work. However, more efforts in theory or simulation are needed to bridge the gap between the superdiffusion model and a certain physical process such as the particle transport in relic PWNe.

ACKNOWLEDGMENTS

We thank Professor Si-Ming Liu for the discussion, which is an incentive for this work. This work is supported by the National Key Program for Research and Development (No. 2016YFA0400200) and by the National Natural Science Foundation of China under Grants No. U1738209 and No. 11851303.

[1] A. Abeysekara *et al.* (HAWC Collaboration), Science **358**, 911 (2017).
[2] M. Di Mauro, S. Manconi, and F. Donato, Phys. Rev. D **101**, 103035 (2020).
[3] G. Giacinti, A. Mitchell, R. López-Coto, V. Joshi, R. Parsons, and J. Hinton, Astron. Astrophys. **636**, A113 (2020).
[4] B. M. Gaensler and P. O. Slane, Annu. Rev. Astron. Astrophys. **44**, 17 (2006).
[5] K. Fang, X.-J. Bi, and P.-F. Yin, Mon. Not. R. Astron. Soc. **488**, 4074 (2019).
[6] P. A. Caraveo, G. F. Bignami, A. De Luca, S. Mereghetti, A. Pellizzoni, R. Mignani, A. Tur, and W. Becker, Science **301**, 1345 (2003).
[7] G. G. Pavlov, D. Sanwal, and V. E. Zavlin, Astrophys. J. **643**, 1146 (2006).
[8] B. Posselt, G. Pavlov, P. Slane, R. Romani, N. Bucciantini, A. Bykov, O. Kargaltsev, M. Weisskopf, and C. Y. Ng, Astrophys. J. **835**, 66 (2017).
[9] V. L. Ginzburg and S. I. Syrovatskii, *The Origin of Cosmic Rays* (Macmillan, New York, 1964).
[10] A. A. Lagutin, Y. A. Nikulin, and V. V. Uchaikin, Nucl. Phys. B, Proc. Suppl. **97**, 267 (2001).
[11] A. A. Lagutin and V. V. Uchaikin, Nucl. Instrum. Methods Phys. Res., Sect. B **201**, 212 (2003).
[12] V. V. Uchaikin and R. T. Sibatov, Gravitation Cosmol. **18**, 122 (2012).
[13] V. Uchaikin and R. Sibatov, arXiv:1703.06486.
[14] N. Volkov, A. Lagutin, and A. Tyumentsev, J. Phys. Conf. Ser. **632**, 012027 (2015).
[15] S. Perri, E. Amato, and G. Zimbardo, Astron. Astrophys. **596**, A34 (2016).
[16] G. Zimbardo and S. Perri, Mon. Not. R. Astron. Soc. **478**, 4922 (2018).
[17] K. Fang, X.-J. Bi, S.-J. Lin, and Q. Yuan, Chin. Phys. Lett. **38**, 039801 (2021), http://cpl.iphy.ac.cn/10.1088/0256-307X/38/3/039801.
[18] V. V. Uchaikin and V. M. Zolotarev, *Chance and Stability* (VSP, Utrecht, Netherlands, 1999).
[19] G. Blumenthal and R. Gould, Rev. Mod. Phys. **42**, 237 (1970).
[20] M. Aguilar *et al.* (AMS Collaboration), Phys. Rev. Lett. **117**, 231102 (2016).
[21] C. Evoli, T. Linden, and G. Morlino, Phys. Rev. D **98**, 063017 (2018).
[22] R.-Y. Liu, H. Yan, and H. Zhang, Phys. Rev. Lett. **123**, 221103 (2019).
[23] R. N. Manchester, G. B. Hobbs, A. Teoh, and M. Hobbs, Astron. J. **129**, 1993 (2005).
[24] P. A. Caraveo, G. F. Bignami, R. Mignani, and L. G. Taff, Astrophys. J. Lett. **461**, L91 (1996).
[25] J. Faherty, F. M. Walter, and J. Anderson, Astrophys. Space Sci. **308**, 225 (2007).
[26] M. Powell, Technical Report No. NA06, Department of Applied Mathematics and Theoretical Physics, 2009, http://www.damtp.cam.ac.uk/user/na/NA_papers/NA2009_06.pdf.
[27] A. A. Dubkov, B. Spagnolo, and V. V. Uchaikin, Int. J. Bifurcation Chaos Appl. Sci. Eng. **18**, 2649 (2008).
[28] D. Hooper, P. Blasi, and P. D. Serpico, J. Cosmol. Astropart. Phys. 01 (2009) 025.
[29] H. Yuksel, M. D. Kistler, and T. Stanev, Phys. Rev. Lett. **103**, 051101 (2009).
[30] P.-F. Yin, Z.-H. Yu, Q. Yuan, and X.-J. Bi, Phys. Rev. D **88**, 023001 (2013).
[31] D. Hooper, I. Cholis, T. Linden, and K. Fang, Phys. Rev. D **96**, 103013 (2017).
[32] K. Fang, X.-J. Bi, P.-F. Yin, and Q. Yuan, Astrophys. J. **863**, 30 (2018).
[33] S. Profumo, J. Reynoso-Cordova, N. Kaaz, and M. Silverman, Phys. Rev. D **97**, 123008 (2018).
[34] X. Tang and T. Piran, Mon. Not. R. Astron. Soc. **484**, 3491 (2019).
[35] J. Feng, N. Tomassetti, and A. Oliva, Phys. Rev. D **94**, 123007 (2016).
[36] Y.-Q. Guo and Q. Yuan, Phys. Rev. D **97**, 063008 (2018).
[37] M. Aguilar *et al.* (AMS Collaboration), Phys. Rev. Lett. **122**, 041102 (2019).
[38] S.-Q. Xi, R.-Y. Liu, Z.-Q. Huang, K. Fang, and X.-Y. Wang, Astrophys. J. **878**, 104 (2019).
[39] M. Di Mauro, S. Manconi, and F. Donato, Phys. Rev. D **100**, 123015 (2019).
[40] J. M. Blondin, R. A. Chevalier, and D. M. Frierson, Astrophys. J. **563**, 806 (2001).